The Measurement and Parameterization of Effective Radius of Droplets in Warm Stratocumulus Clouds

G. M. MARTIN, D. W. JOHNSON, AND A. SPICE

U.K. Meteorological Office, Meteorological Research Flight, Farnborough, Hampshire, England

(Manuscript received 15 March 1993, in final form 12 November 1993)

ABSTRACT

Observations from the Meteorological Research Flight's Hercules C-130 aircraft of the microphysical characteristics of warm stratocumulus clouds have been analyzed to investigate the variation of the effective radius of cloud droplets in layer clouds. Results from experiments in the eastern Pacific, South Atlantic, subtropical regions of the North Atlantic, and the sea areas around the British Isles are presented. In situations where entrainment effects are small the (effective radius)^3 is found to be a linear function of the (volume-averaged radius)^3 in a given cloud and can thus be parameterized with respect to the liquid water content and the droplet number concentration in the cloud. However, the shape of the droplet size spectrum is very dependent on the cloud condensation nuclei (CCN) characteristics below cloud base, and the relationship between effective radius and volume-averaged radius varies between maritime air masses and continental air masses. This study also details comparisons that have been made in stratocumulus between the droplet number concentrations and (a) aerosol concentrations below cloud base in the size range 0.1 to 3.0 μm and (b) CCN supersaturation spectra in the boundary layer. A parameterization relating droplet concentration and aerosol concentration is suggested. The effects of nonadiabatic processes on the parameterization of effective radius are discussed. Drizzle is found to have little effect near cloud top, but in precipitating stratocumulus clouds the parameterization breaks down near cloud base. Comparisons are made between this parameterization of effective radius and others used currently or in the past.

1. Introduction

Boundary-layer clouds are important components of the earth's energy budget. Stratus and stratocumulus clouds, in particular, have high albedos and reduce the shortwave radiation received at the earth's surface (Albrecht et al. 1988; Betts and Boers 1990). They are observed to occur in very persistent sheets covering large areas of the eastern parts of subtropical ocean basins over the cooler ocean currents found there and as more transient features under midlatitude anticyclones (Schmetz et al. 1983) and in arctic regions (Curry and Herman 1985). The reflectivity of these clouds is very sensitive to their liquid water content and to the microphysical processes going on within them (Taylor and Ghan 1992). Twomey (1974) has suggested that their albedo is modified by the characteristics of the cloud condensation nuclei (CCN) available to form the cloud drops. By changing the droplet size distribution and concentration, the optical properties of the cloud may be altered sufficiently to change the global energy budget and thus the climate (Twomey 1977; Charlson et al. 1987). It is therefore vitally important that numerical weather and climate models simulate realistically the radiative properties of these clouds (Mitchell et al. 1989).

However, such models have too large a grid spacing to resolve explicitly the microphysical processes associated with these clouds. Therefore, their effects have to be parameterized in terms of the bulk model variables in order to improve the model predictions. The three most important parameters needed to describe the radiative properties of clouds are

(i) the optical thickness,
(ii) the single scattering albedo, and
(iii) the asymmetry factor.

Stephens (1978b) and Slingo and Schrecker (1982) show that in liquid water clouds all three of these can be parameterized in terms of the effective radius (r_e) of the droplet size spectrum. The effective radius is defined as the ratio of the third to the second moment of the size spectrum; that is,

$$r_e = \frac{\int_{r=0}^{\infty} N_r r^3 dr}{\int_{r=0}^{\infty} N_r r^2 dr}, \quad (1)$$

where r is the cloud droplet radius and N the droplet

Corresponding author address: Miss G. M. Martin, Meteorological Office, Meteorological Research Flight, Building Y46, DRA Farnborough, Hampshire, GU14 6TD, England.

concentration. Slingo (1990) estimated that decreasing the effective radius of cloud droplets from 10 to 8 μm, which increases the shortwave albedo, would result in atmospheric cooling that could offset global warming due to doubling the CO_2 content of the atmosphere. Equally, Randall et al. (1984) have shown that this offset could also be brought about about by a 4% increase in the area covered by stratocumulus. Radiation schemes used in large-scale numerical models are therefore very sensitive to the effective radius.

Slingo (1989) suggested that the dependence of the cloud radiative properties on the liquid water path and on the droplet effective radius should be considered separately. Using this approach, he derived a parameterization of the shortwave radiative properties of water clouds, which compared well with observations. This showed that for a constant liquid water path, the reflectivity increases with decreasing droplet effective radius, but for a constant effective radius, the reflectivity increases with increasing liquid water path. As the liquid water path increases, however, the influence of both the droplet effective radius and the liquid water path itself on the cloud reflectivity decreases, implying that the sensitivity of the shortwave radiative properties of clouds to changes in microphysics or cloud thickness will be greatest for clouds with liquid water paths between about 10 and 100 g m^{-2}. Fouquart et al. (1990) summarized observations of clouds made in many different locations around the world. According to these observations, the liquid water paths of stratus and stratocumulus clouds range roughly between 10 and 200 g m^{-2}.

At present, most general circulation models use a constant value of r_e for water clouds and another for ice clouds. For example, in the U.K. Meteorological Office unified model the r_e used is 7 μm for water clouds (this has recently been changed from 10 μm) and 30 μm for ice clouds. In the European Centre for Medium-Range Weather Forecasts (ECMWF) operational model, a value of 15 μm is used for water clouds (Morcrette 1990). The Canadian Climate Centre (McFarlane et al. 1992) has attempted to add realism by using a very simple algorithm that relates r_e to the liquid water content (L), that is,

$$r_e\,[\mu\text{m}] = 11L\,[\text{g m}^{-3}] + 4. \qquad (2)$$

This expression was empirically derived by Fouquart et al. (1990) from "standard clouds" described by Stephens (1978a), which range from stratus to cumulonimbus but include cumulus and stratocumulus clouds in both maritime and continental air masses.

In smaller-scale models, attempts have been made to parameterize r_e assuming a droplet spectrum that varies with liquid water content but has a constant shape. Moeng and Curry (1990), in a large eddy simulation of stratus clouds, used a Khrgian–Mazin drop size distribution,

$$n(r) = ar^2e^{-br}, \qquad (3)$$

where n is concentration, r drop radius, and a and b are functions of liquid water content. The r_e can then be explicitly calculated. Jonas (1990) found that in a one-dimensional model of the growth of droplets by condensation in an entraining warm cumulus cloud, the r_e of the droplet spectrum was dependent on the CCN spectrum and the liquid water content, but was relatively insensitive to other properties of the cloud. However, Bower and Choularton (1992), when they analyzed measurements of the microphysical properties of continental cumulus, small cumulus and stratiform cloud around the United Kingdom, and subtropical marine stratocumulus, found that the fundamental differences in entrainment processes associated with layer and convective clouds produced differences in the droplet size spectra, which necessitated separate parameterizations of r_e for these cloud types. They observed that in convective clouds, away from cloud base, the entrainment is strong enough that the r_e varies very little throughout the depth of the cloud; so it is possible to parameterize r_e as a constant in cumuli that has one value over land (10 μm) and a larger value (14 μm) over the sea. For layer cloud, empirical parameterizations were produced relating r_e to liquid water content and droplet concentration where the droplet concentrations were set to constant values typical of maritime and continental clouds. Pontikis and Hicks (1992) have studied data from penetrations of maritime cumuli during the Joint Hawaii Warm Rain Project (JHWRP). They derived an analytical expression for r_e related to the dispersion of the droplet spectra (see section 3 for definition) as well as the liquid water content of the cloud and the droplet concentration. They found that their experimental results compared favorably with this. Blyth and Latham (1991), using aircraft measurements in cumulus clouds in Montana (during the Cooperative Convection Precipitation Experiment, CCOPE) and New Mexico, have suggested that r_e in cumulus clouds can be parameterized using the adiabatic liquid water content and the maximum droplet number concentration $N_{\max}$, but were unable to find a suitable way of parameterizing $N_{\max}$ in a large scale numerical model.

The main focus of this paper is the analysis of extensive aircraft observations of stratocumulus clouds from several different regions of the world in both maritime air masses (that is, air that had traveled a significant distance over the sea) and continental air masses (that is, air that had recently passed over land), which suggest a new parameterization of effective radius for layer clouds that could be used in numerical model radiation schemes. The instrumentation and datasets used are described in section 2. The general characteristics of stratocumulus clouds and their droplet spectra found during the course of the experiments are shown in section 3, and section 4 details the parameterization of r_e suggested by the results. In section 5, the parameter-

ization is compared with others used in the past, and its limitations are discussed.

2. Instrumentation and datasets used

The results described below were obtained using data gathered by the Meteorological Research Flight (MRF) Hercules C-130 aircraft during

(i) the First ISCCP (International Satellite Cloud Climatology Program) Regional Experiment (FIRE) conducted over the eastern Pacific Ocean off the southern coast of California in July 1987,

(ii) the First ATSR (Along Track Scanning Radiometer) Tropical Experiment (FATE) in the South Atlantic during November 1991,

(iii) flights made in stratocumulus over the sea areas around the British Isles between December 1990 and February 1992, and

(iv) the Atlantic Stratocumulus Transition Experiment (ASTEX) carried out in the North Atlantic in the vicinity of the Azores in June 1992.

In all, data from 35 flights have been used.

The C-130 aircraft is well equipped to measure the radiative and microphysical properties of stratocumulus clouds, and detailed information about the instrumentation and its performance is given in Nicholls (1978). The instruments used to obtain the microphysical data analyzed here were a Particle Measuring System (PMS) Passive Cavity Aerosol Spectrometer Probe (PCASP), which measures aerosol particles in the range 0.05 to 1.50 μm radius, a PMS Forward Scattering Spectrometer Probe (FSSP), which measures droplets in the range 0.25 to 24 μm radius, and a PMS 2D cloud probe, which measures droplets in the size range 12.5 to 400 μm radius (Baumgardner 1989). A thermal gradient diffusion chamber was used to measure CCN activity spectra (Saxena and Kassner 1970).

Regular maintenance and calibration of the PMS probes are carried out in order to minimize the potential measurement errors associated with these instruments. Standard corrections such as the calculation of the effective beam diameter and the activity correction (Baumgardner 1983) are applied to the FSSP concentration measurements, and the activity correction is also applied to the PCASP concentration measurements. Baumgardner (1983) presents an analysis of the estimated accuracy in the measured FSSP concentrations when these corrections are applied compared with the accuracy when they are not applied. The average uncertainty is reduced from 45%–100% to 17% when the corrections are applied. Sizing errors in the FSSP are kept to a minimum by regular calibrations using glass microspheres. However, uncertainties are thought to be introduced by laser inhomogeneity (Baumgardner and Spowart 1990), coincidence of droplets in the beam (Cooper 1988), and the limited response time of the probe's electronics (Baumgardner and Spowart 1990). Such errors are estimated (Baumgardner 1983) to result in an average sizing uncertainty of 17%.

Strapp et al. (1992) discussed possible errors in the PCASP measurements due to drying of hydrated aerosol particles by the probe's deicing heaters, which are normally operated continuously, even in nonicing conditions. They found that the spectral shape was altered due to drying of hydrated aerosol particles. All of the measurements made by the PCASP in this study were with the deicing heaters switched on. However, since only the total particle concentration measurements from the PCASP have been used in this study, rather than the particle size spectra, the results should not be affected.

In general, two basic flight patterns were used in this study: (a) a profile where a slow descent (500 ft/min in the boundary layer, 1000 ft/min in the free troposphere) was made through the cloud sampling the microphysics of the cloud and the aerosol characteristics below cloud base, and (b) a stack in which a series of 5 to 10 minute straight and level runs was performed, the first immediately below the cloud base to sample the aerosol in the boundary layer and the rest at several different heights in the cloud. Frequently, the aerosol characteristics of the free tropospheric air were measured with a straight and level run above the cloud. As the diffusion chamber required the sample air to be at aircraft cabin temperature, outside air had to be taken into the aircraft through a Global Atmospheric Sampling Programme (GASP) probe (Perkins and Gustafsson 1975) and into an alleviator where a neoprene bladder was used to pressurize the sample to cabin pressure. The alleviator was large enough for several samples to be extracted from it so that CCN supersaturation spectra could be determined. Unfortunately, this technique is very slow, so normally only one CCN supersaturation spectrum could be obtained below cloud base in both the profiles and the stacks.

3. Characteristics of stratocumulus cloud

Stratocumulus clouds normally form underneath a subsidence inversion in a boundary layer with a reasonable supply of moisture, such as over the sea. Figure 1a shows a typical temperature and dewpoint profile obtained during a slow descent through a layer of stratocumulus off the coast of California. In this case the subtropical high was well to the west of California and the cloud had formed in a moderate northerly flow. The boundary layer, which was well mixed, as indicated by the equivalent potential temperature profile (Fig. 1b), was approximately 1 km deep and capped by a sharp temperature inversion and a cloud layer that was 400 m thick (the spike in this profile near the cloud top is the result of a lag of the General Eastern dewpoint hygrometer, which occurs when sharp changes in dewpoint are encountered). As found by several other investigators (Nicholls 1984; Nicholls and Leighton

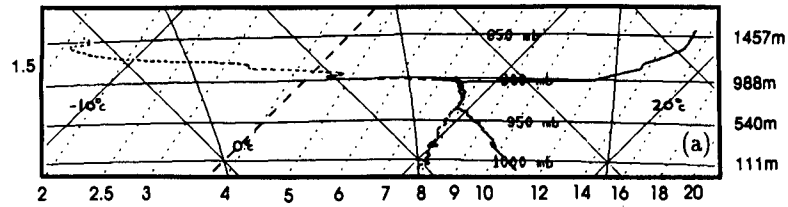

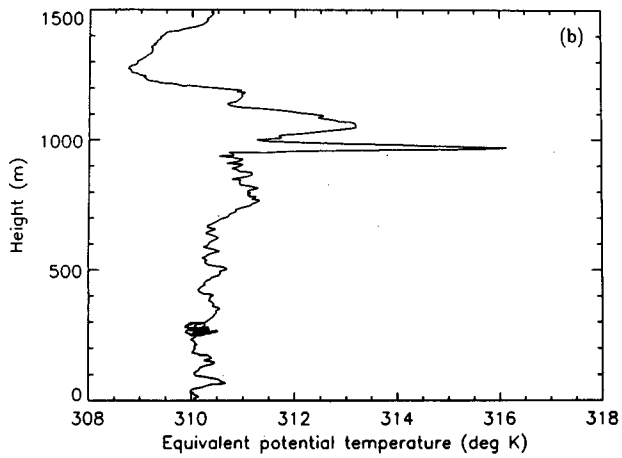

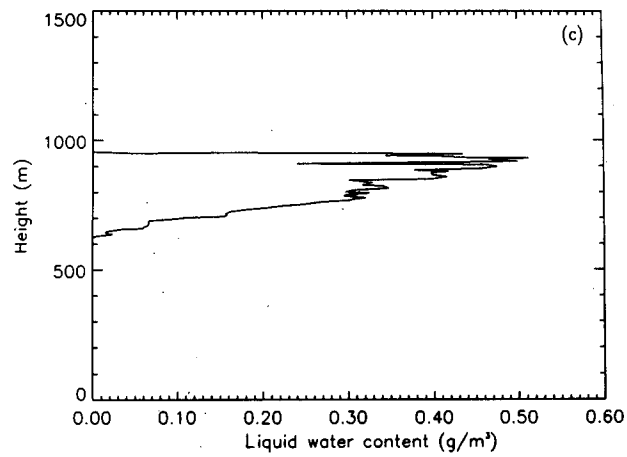

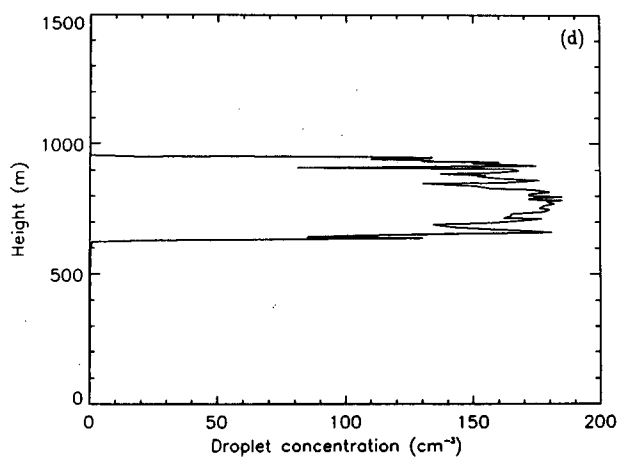

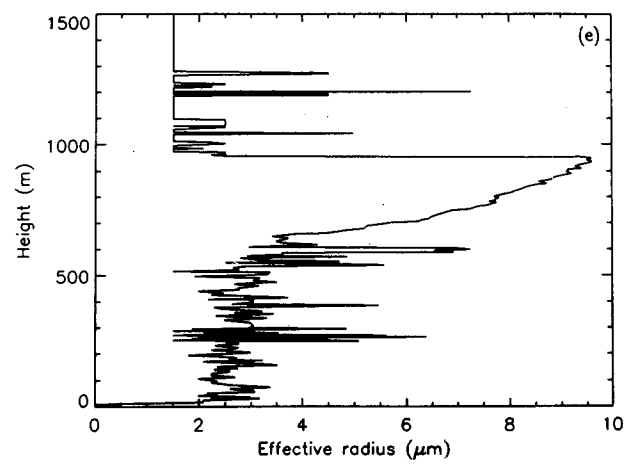

FIG. 1. Profiles obtained through a stratocumulus layer in a maritime airmass during FIRE on 3 July 1987 of (a) temperature (°C, solid line) and dewpoint (°C, dashed line) plotted on a tephigram [dotted lines are humidity mixing ratio (g kg^{-1}); height at each pressure level is referenced to a mean sea level pressure of 1013.25 mb], (b) equivalent potential temperature (K), (c) liquid water content (g m^{-3}) as measured by the FSSP, (d) cloud droplet concentration (cm^{-3}), and (e) effective radius (μm) [values of r_e measured when out of cloud are due to noise in the first channel of the FSSP].

1986; Albrecht et al. 1988; Bower and Choularton 1992), the corresponding liquid water content profile, as shown in Fig. 1c, increases smoothly with height, with a large step change at cloud top. However, the droplet concentration (Fig. 1d) measured by the FSSP remains almost constant throughout the depth of the cloud, and there are sharp changes both at cloud base and cloud top. The average size of the droplets increases with height, as illustrated in Fig. 1e, which is a profile of the effective radius of cloud droplets. This is calculated from droplet size spectra measured by the FSSP using the following equation [which is a finite version of Eq. (1)]:

$$r_e = \frac{\sum_{n=1}^{M} r_n^3 N_n}{\sum_{n=1}^{M} r_n^2 N_n}, \qquad (4)$$

where M is the number of size bins resolved by the FSSP ($M = 15$), r_n is the middle radius value for that size bin, and N_n is the concentration of droplets in that size bin.

Figure 2a–c shows the typical variation of liquid water content, effective radius, and droplet concentration observed in a straight and level run in the stratocumulus ayers used in this study. In this particular case, the experiment was carried out in the southwest approaches to the British Isles, at a height of 1000 m, quite close to the top of a layer of stratocumulus 200 m thick. Along the 30-km run the effective radius varies by less than 1.0 μm and the mean concentration slowly decreases by about 30 cm^{-3}.

The examples given in Figs. 1 and 2 are typical of most of the stratocumulus clouds used in this study. They are consistent with a layer of cloud having formed in a boundary layer with relatively homogeneous aerosol characteristics just below cloud base and where the maximum supersaturation in the rising parcels of air is experienced just above cloud base, so that all the CCN in the parcel that are going to be activated are activated at this level. Therefore, the droplet concentration remains constant throughout the depth of the cloud. Occasionally, profiles showed a decrease in mean droplet concentration close to the upper and lower cloud boundaries, with corresponding decreases in liquid water content. However, in most cases these effects were small, which indicates that entrainment in these stratocumulus clouds is not generally a significant effect and is mainly limited to cloud top. This was also found in studies by Nicholls and Leighton (1986) and Bower and Choularton (1992). On occasions when entrainment was noticeable, such as when cumulus clouds were penetrating the layer or when the layer was very thin or broken, the data were left out of the analysis.

The difference in shape of the droplet spectra from maritime and continental airmass clouds was the most significant microphysical variation observed in the stratocumulus clouds during the course of these experiments. The airmass type in each case was determined by referring to the synoptic situation and deciding whether or not the air would have recently passed over land. For a large majority of the time during FIRE and FATE, relatively clean maritime air masses were encountered since in each case the air had traveled a considerable distance over the ocean. During the flights around the United Kingdom, apart from a few exceptional cases, nearly all air masses showed the effects of continental sources; even short tracks across land, such as a west to northwesterly flow over southern Ireland, considerably modified the aerosol characteristics. When typical spectra from around the United Kingdom are compared with those from off the coast of California, quite large differences are found. During ASTEX, even though the Azores are a long way from the European continent, a wide variety of air masses were sampled. Those coming predominantly from the north or northwest were relatively clean, but strong east to northeast outflows from Europe were found to be very polluted on several occasions. There were marked differences in the shape of the droplet spectra measured in these air masses.

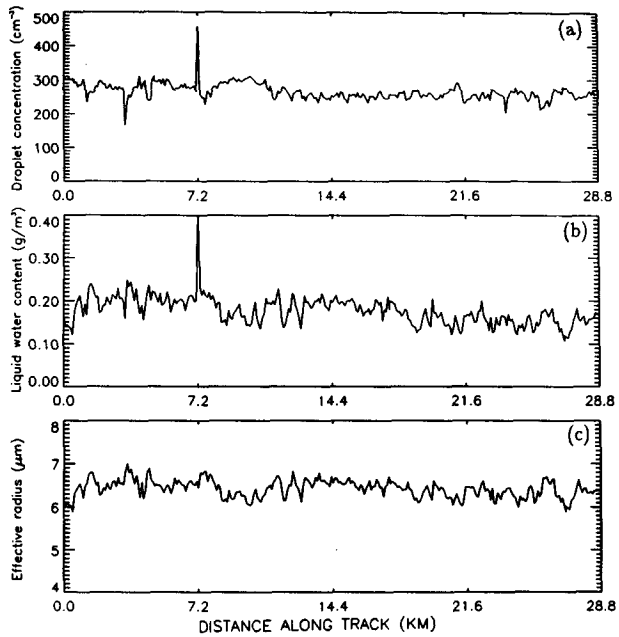

FIG. 2. Time series during a straight and level run in the top of a stratocumulus layer in a continental air mass over the sea to the southwest of the British Isles on 5 February 1992 of (a) cloud droplet concentration (cm^{-3}), (b) liquid water content (g m^{-3}) as measured by the FSSP, and (c) r_e (μm).

Figure 3a shows a typical set of averaged droplet size spectra for a layer of stratocumulus sampled during FATE in a maritime air mass. The peak concentration in the cloud remains almost constant with height but the proportion of larger droplets increases, causing a

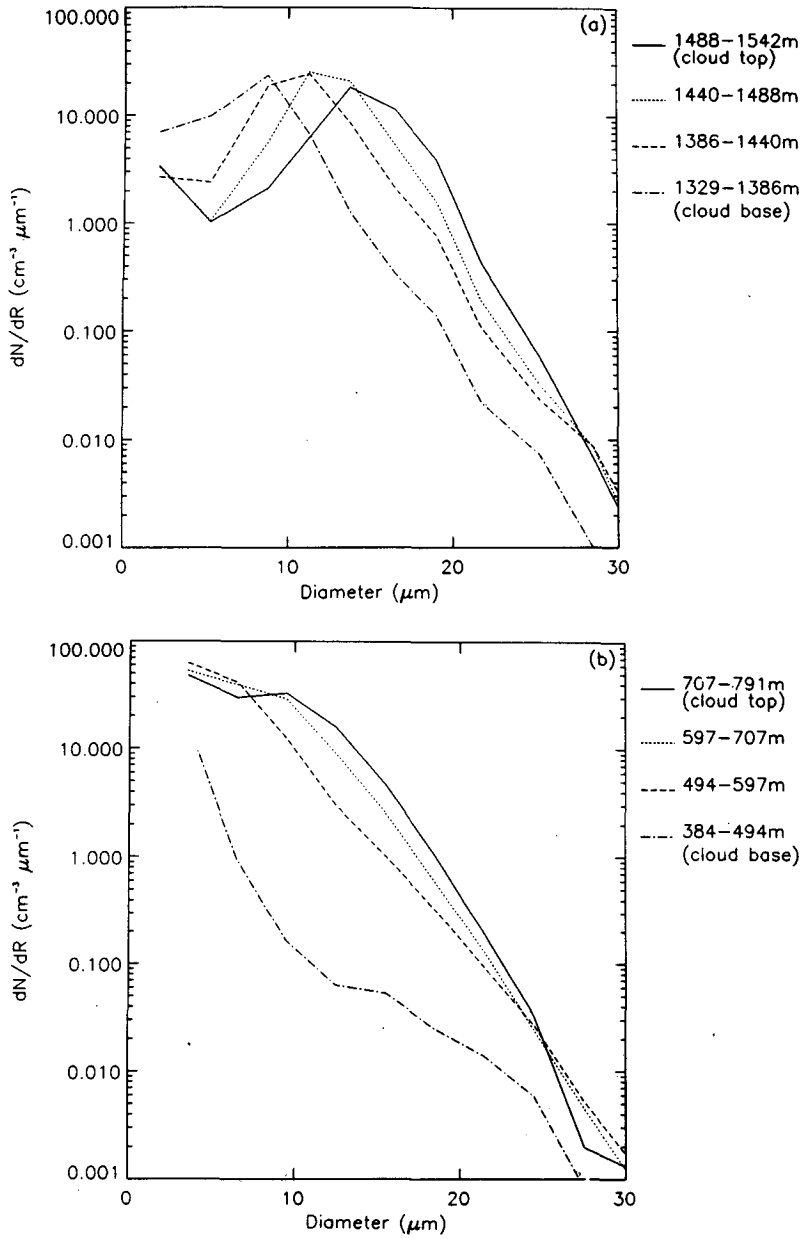

FIG. 3. Droplet size spectra measured by the FSSP in stratocumulus layers during profiles in (a) a maritime air mass from FATE on 6 November 1991 and (b) a continental air mass over the North Sea on 26 February 1991.

significant movement of the peak to larger radii. Thus, the effective radius increases with height in cloud. A set of droplet spectra from a cloud layer sampled around the United Kingdom in a continental air mass is shown in Fig. 3b. This also shows an increase in average droplet size toward the cloud top, but the shapes of the spectra are very different from those in Fig. 3a. The peak size of the droplets at cloud top is smaller than in the maritime case, but there are still significant numbers of droplets in the larger size ranges and as a result the spectra are more skewed.

The differences in spectral shape may be compared quantitatively using spectral dispersion (d), which is the ratio of the standard deviation σ of the spectrum to the mean radius ($\bar{r}$); that is,

$$d = \frac{\sigma}{\bar{r}}. \tag{5}$$

This can be calculated for each one-second record of a vertical profile through cloud, and is shown in Fig. 4 as a function of normalized height above cloud base,

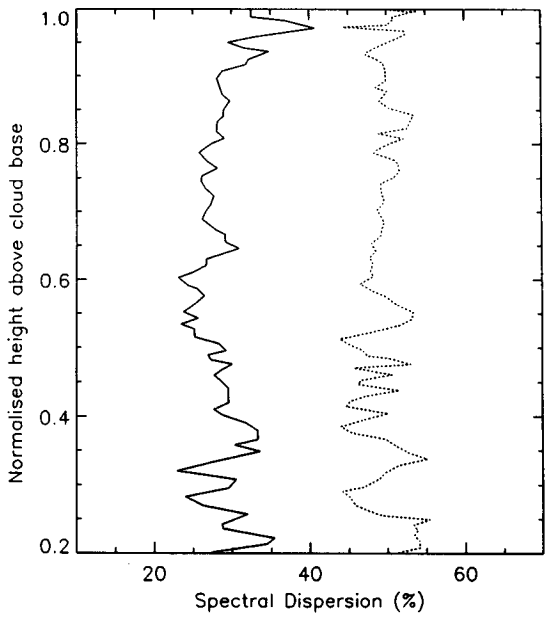

FIG. 4. A plot of spectral dispersion (d) against normalized height in stratocumulus cloud in a maritime air mass (solid line) during FATE on 6 November 1991 and a continental air mass (dashed line) over the North Sea on 26 February 1991.

for the spectra given in Figs. 3a and 3b. The difference in spectral dispersion for the two cases can be seen clearly. Note, however, that two spectra that have the same dispersion are not necessarily the same shape, so that dispersion alone cannot be used to distinguish between airmass types in this way. This method has been used here simply to illustrate the differences between the two cases. It is interesting also to notice that the dispersion is approximately constant with height, because this indicates that the spectrum must broaden as the mean droplet size increases [see Eq. (5)]. This was also observed by Nicholls and Leighton (1986).

4. A parameterization for the effective radius of cloud droplets

a. Theoretical basis

The liquid water content can be calculated from a particular droplet size spectrum using the following equation:

$$L = \frac{4}{3}\pi\rho_w \int_0^\infty Nr^3 dr, \tag{6}$$

where L is the mass of liquid water per unit volume of air. The FSSP has 15 size channels, so this equation can be approximated by the summation:

$$L = \frac{4}{3}\pi\rho_w \sum_{n=1}^{15} r_n^3 N_n, \tag{7}$$

where N_n denotes the concentration of droplets in the size range n, r_n the radius of droplets in that size range, and ρ_w the density of liquid water. This can be expressed as

$$L = \frac{4}{3}\pi\rho_w \overline{r^3} N_{\mathrm{TOT}}, \tag{8}$$

where N_{TOT} is the total droplet concentration. The quantity $\frac{4}{3}\pi\overline{r^3}$ in this equation is the average volume of a droplet in the spectrum, so that

$$r_v = (\overline{r^3})^{1/3} \tag{9}$$

is the mean volume radius (a common measure of average droplet radius derived from size spectra).

b. Relationship between r_e and r_v

If a relationship can be found between r_e and r_v then Eq. (8) can be used as a starting point for a parameterization of r_e in terms of the liquid water content of the cloud and the droplet concentration. Bower and Choularton (1992) compared r_v with r_e for a descent through stratocumulus during one of the FIRE flights and found that r_v was consistently lower than r_e by about 1 μm. However, the results presented in this paper indicate that there is a linear relationship between r_v^3 and r_e^3 in stratocumulus clouds where little entrainment is going on. That is,

$$r_v^3 = kr_e^3, \tag{10}$$

where k is a constant.

Figure 5a shows a typical example of a scatterplot of 1-sec averages of r_v^3 against r_e^3 measured by an FSSP in a profile through a layer of stratocumulus 250 m thick. A very good straight line that passes through the origin is found with little scatter. This particular case was for a maritime air mass studied during FIRE where the maximum average droplet sizes were large. Figure 5b is for a stratocumulus sheet 490 m thick in a continental air mass found in the southwest approaches to the United Kingdom. Note that the maximum average droplet size is much smaller, even though the cloud is thicker; the graph is plotted on a different scale. Once again a straight line, with little scatter, passing through the origin results but the gradient (k) of the line is smaller. Similar scatterplots were produced for all profiles through cloud in these experiments, and it was found consistently that k varied with airmass type. In the maritime air masses sampled in FIRE, FATE, ASTEX, and around the United Kingdom, larger values of k were measured than in the continental air masses found in the vicinity of the United Kingdom and during ASTEX. This arises because of the fundamental difference in the shape of the droplet size spectra, which was discussed in the previous section for the two airmass types. In continental air masses it was found that $k = 0.67 \pm 0.07$ (one standard deviation) while in the maritime air masses $k = 0.80 \pm 0.07$.

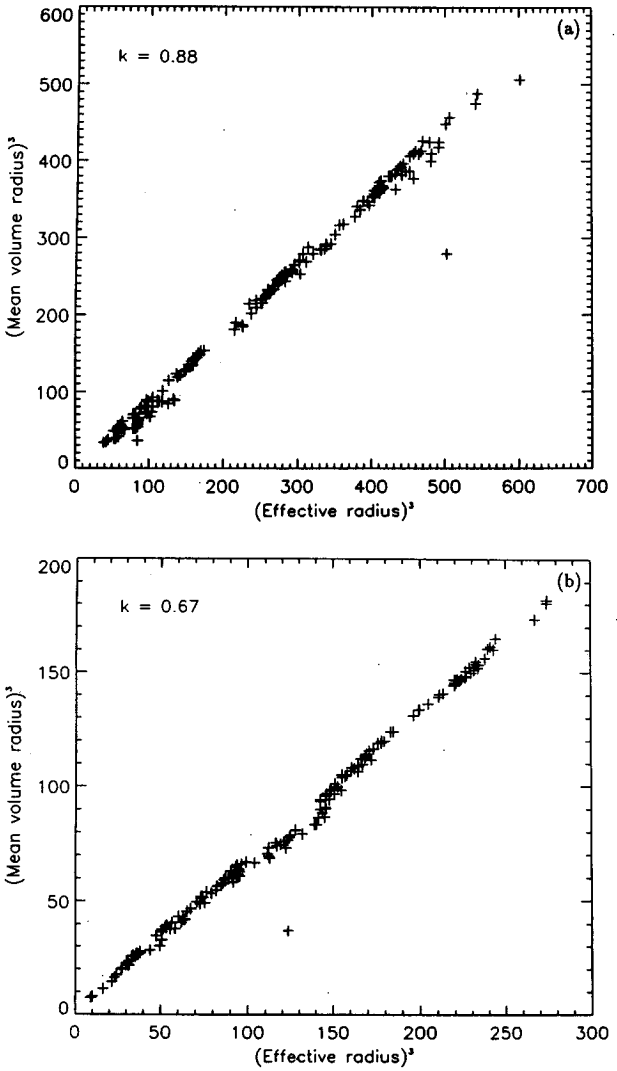

FIG. 5. Scatterplots of r_v^3 (μm^3) against r_e^3 (μm^3) for (a) a maritime airmass cloud during FIRE on 13 July 1987 and (b) a continental airmass cloud over the southwest approaches to the British Isles on 6 December 1990.

It is suggested that a suitable parameterization for effective radius is

$$r_e = \left(\frac{3L}{4\pi\rho_w k N_{\mathrm{TOT}}}\right)^{1/3}. \qquad (11)$$

The results from all the flights are summarized schematically in Fig. 6, where r_e^3 is plotted against L/N_{TOT} (FSSP liquid water content/droplet concentration). The graph shows the spread of scatterplot gradients (± 1 standard deviation) and they fall into two separate regions: one for continental air masses and the other for maritime air masses. Also plotted on the graph is a line for $r_e^3 = r_v^3$ that represents $k = 1$.

c. *Effect of aerosol on cloud droplet concentration*

1) RELATIONSHIP BETWEEN CLOUD DROPLET CONCENTRATION AND AEROSOL CONCENTRATION

Cloud droplet concentration is a difficult parameter for a large-scale numerical model to handle due to its transient and subgrid-scale nature. Therefore, before Eq. (11) can be used to diagnose effective radius in models, a method for parameterizing N_{TOT} is required. In stratocumulus clouds, in well-mixed boundary layers, the droplet concentration throughout the whole depth of the cloud is almost equal to the CCN concentration below cloud, and therefore in a maritime air mass it would be expected that the droplet concentration would be much less than in continental air masses. Thus, N_{TOT} could be approximated by choosing a characteristic value for a given air mass, where the airmass type is determined by whether the air is over the land or over the sea. Bower and Choularton (1992) used $N_{\mathrm{TOT}} = 600$ cm^{-3} over the continents and $N_{\mathrm{TOT}} = 150$ cm^{-3} over the sea.

However, this simple scheme would lead to a value of r_e that would often be in error since continental-type air masses are often observed to retain their high aerosol content for some distance over the sea. As numerical models become more sophisticated, it is likely that a predictive aerosol parameter will need to be included. It is well known that the concentration and chemical characteristics of aerosol particles will directly affect the concentration and maximum size of cloud droplets forming in an air mass, and hence will affect the cloud optical thickness and albedo (Twomey 1974, 1977). Thus, the inclusion of such a variable would be advantageous both from the point of view of radiation

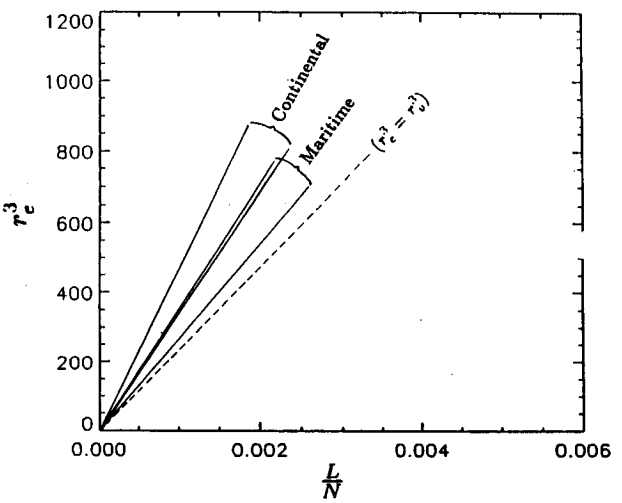

FIG. 6. Summary of the range of gradients (± 1 standard deviation) in maritime and continental airmass clouds of r_e^3 (μm^3) against [liquid water content (g m^{-3})/droplet concentration (cm^{-3})] for all the flights. The dashed line $r_e^3 = r_v^3$ represents $k = 1$.

schemes and for predicting visibility. The U.K. mesoscale model (Golding 1990) already has the facility of including an aerosol variable, and investigations are beginning into how aerosol may be included in GCMs (Langner et al. 1992). Figures 7a and 7b show profiles of aerosol concentration measured by the PCASP in a maritime and a continental air mass. It can be seen that the aerosol concentration below cloud in the maritime air mass is much lower than in the continental air mass. The extent to which the aerosol close to the surface affects the cloud droplet concentration will depend on how well mixed the boundary layer is. In Fig. 7a the aerosol concentration is almost constant with height within the boundary layer, indicating that it is well mixed. However, if the surface layer is decoupled from the cloud layer then the concentration may vary with height, as is seen in Fig. 7b, where more aerosol is trapped in the surface layer than in the subcloud layer. Therefore, from the point of view of determining the effect of the aerosol on the cloud, it is important that only the aerosol characteristics in the region just below the cloud base are considered. Normally, the aerosol characteristics above the stable temperature inversion, in the free troposphere, vary significantly from that in the boundary layer. This can be seen clearly in Fig. 7b and to a lesser extent in Fig. 7a.

Aerosol concentration measurements taken with the PCASP during this study show that there is a good correlation between the number of aerosol just below cloud base and the cloud droplet concentration (which, provided there is no input of extra CCN by entrainment or loss of droplets by drizzle, will be the same as the CCN concentration activated into cloud droplets at the cloud base). Figure 8a summarizes the aerosol concentrations measured below cloud base and the number of droplets observed in the cloud for all the UK and FATE flights (the PCASP was not fitted during FIRE). Each point represents the average droplet concentration measured during a profile through a particular layer of cloud compared with the average aerosol concentration measured just below the base of the layer. For the maritime air masses, there is little scatter of the points and the best-fit line is close to the dashed $y = x$ line, indicating that nearly all the aerosol are good CCN and that there is very little variation in the chemical characteristics of the particles. Note that because the lower measurement limit of the PCASP is 0.05 μm, some smaller aerosol particles (including CCN) are likely to be missed, so that the aerosol concentration measured by the PCASP is probably an underestimate of the total aerosol concentration. This would account for the points that lie above the $y = x$ line. However, it is also possible that some processing or scavenging of the aerosol below cloud base by drizzle has taken place.

For the continental air masses the scatter is much larger than for the maritime air masses, illustrating the range of propensities to become CCN and hence the diversity of aerosol chemical characteristics among the air masses sampled. The best line fit to all of the continental airmass data shown in Fig. 8a, if extrapolated to the x axis, would have a positive intercept, which shows that a certain proportion of the continental par-

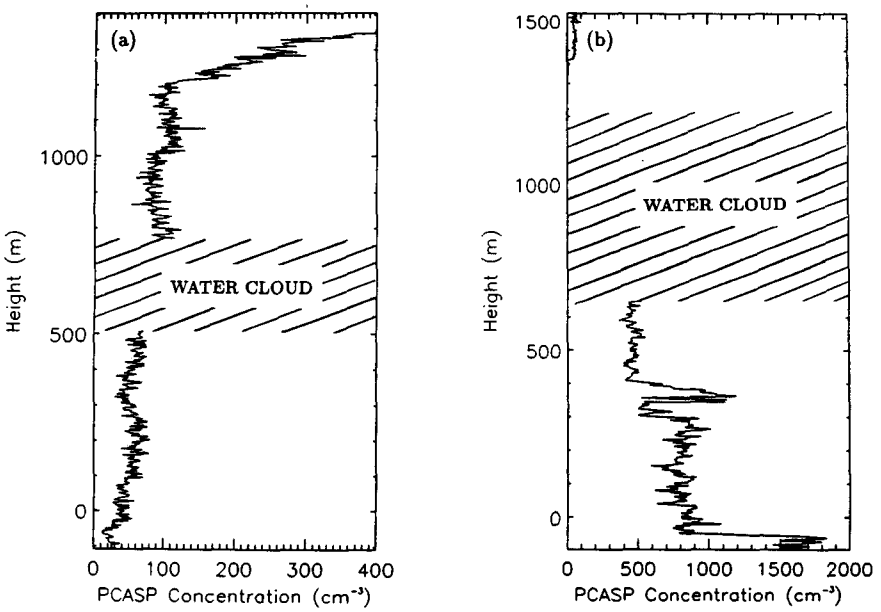

FIG. 7. Vertical profiles of aerosol concentration (cm^{-3}) as measured by the PCASP in (a) a maritime air mass during ASTEX on 16 June 1992 and (b) a continental air mass over the southwest approaches to the British Isles on 6 December 1990. Each profile is plotted against pressure height, which is referenced to a mean sea level pressure of 1013.25 mb.

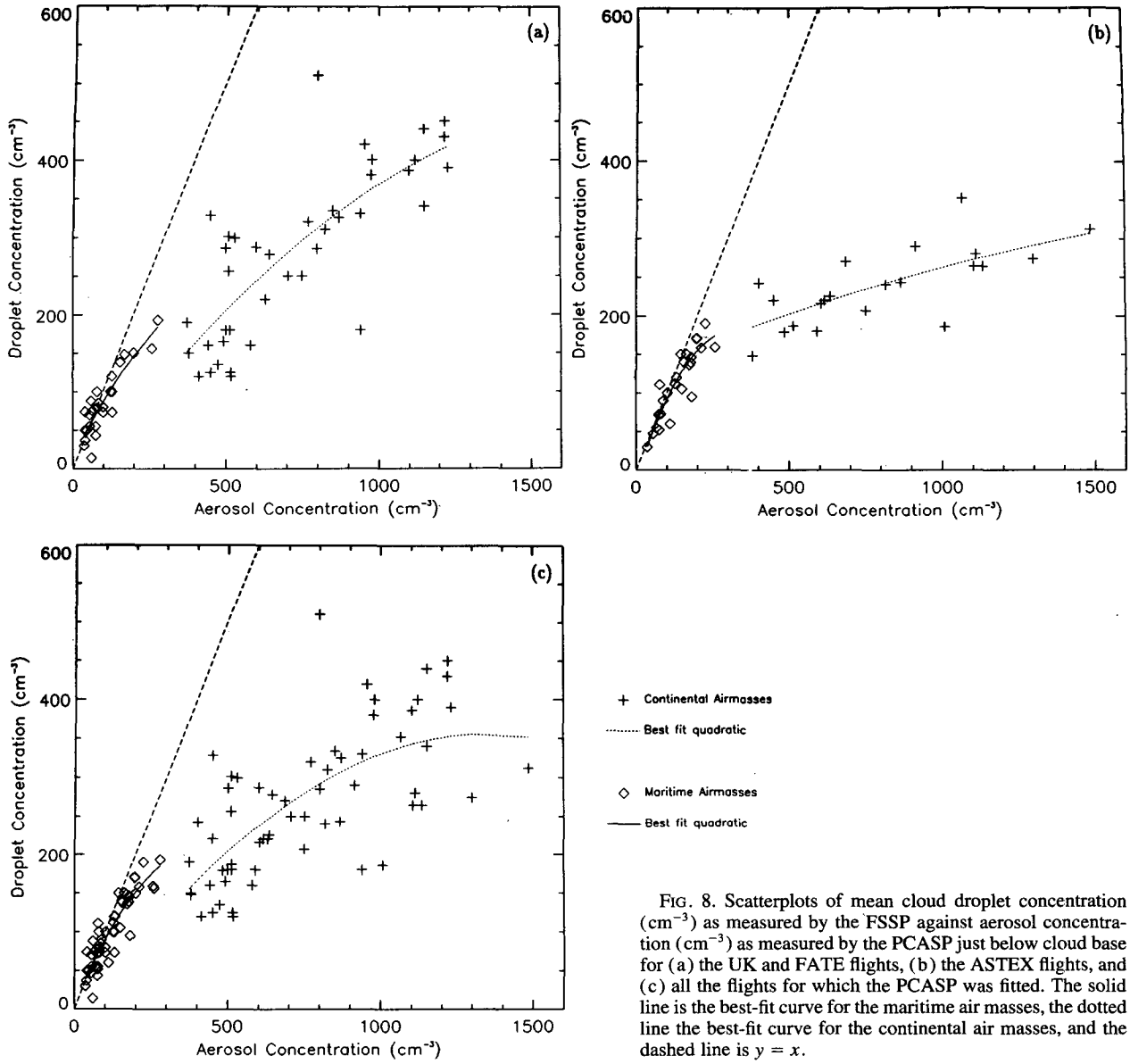

FIG. 8. Scatterplots of mean cloud droplet concentration (cm^{-3}) as measured by the FSSP against aerosol concentration (cm^{-3}) as measured by the PCASP just below cloud base for (a) the UK and FATE flights, (b) the ASTEX flights, and (c) all the flights for which the PCASP was fitted. The solid line is the best-fit curve for the maritime air masses, the dotted line the best-fit curve for the continental air masses, and the dashed line is $y = x$.

ticles are hydrophobic and so will not form cloud droplets. The value of this intercept will vary with the origin of the air mass; for example, an air mass of urban origin would contain a large percentage of anthropogenic aerosol particles such as carbon, which is insoluble, so the relationship between aerosol and CCN concentration for this air mass would differ from one that had, for example, originated over the desert.

It is possible that some of the scatter in Fig. 8a is due to variations in the maximum ambient supersaturation encountered by the CCN entering the cloud base, which would result from variations in the vertical velocity. However, the vertical velocities associated with stratocumulus clouds are very small (typically less than ~ 0.5 m s^{-1}) and are consequently extremely difficult to measure with an aircraft. Thus, it was not possible to relate the scatter of the points in Fig. 8a to variations in the vertical velocity with any confidence. However, it is thought that since the vertical velocities are small, variations in the characteristics of the air masses in which the clouds form will have a greater effect on the cloud droplet concentrations. This is discussed further in the next section.

Figure 8b shows the results for the ASTEX flights. Again, the best-fit line to the maritime airmass data approximates to the $y = x$ line and the scatter is small. However, the best-fit line to the continental airmass data is quite different from that in Fig. 8a. In fact, the two best-fit lines in Fig. 8b are almost continuous. This indicates that the continental air masses in the ASTEX

region with aerosol concentrations below about 600 cm^{-3} have been modified during their comparatively long sea track such that the percentage of hygroscopic particles has been increased. At larger aerosol concentrations, the ratio of activated CCN to total aerosol is smaller than in Fig. 8a, indicating that the origin of the continental air masses in the ASTEX region is different from those around the United Kingdom, and may suggest some Saharan influence.

It follows that if the chemical compositions of each of the air masses sampled in this study were known, a series of curves relating N_{TOT} to aerosol concentration could be drawn that would each represent a characteristic air mass. However, both of these sets of data show that a knowledge of the aerosol concentration in the boundary layer and of the aerosol source can give a reasonable estimation of the cloud droplet concentration in stratocumulus clouds. Figure 8c shows the combined results from all the flights. The best line fits suggest that N_{TOT} can be parameterized in the following manner:

In maritime air masses,

$$N_{TOT} = -1.15 \times 10^{-3}A^2 + 0.963A + 5.30 \quad (12)$$

for values of A in the range ($36 \leq A \leq 280$ cm^{-3}), and in continental air masses

$$N_{TOT} = -2.10 \times 10^{-4}A^2 + 0.568A - 27.9 \quad (13)$$

for values of A in the range ($375 \leq A \leq 1500$ cm^{-3}), where A is the aerosol concentration in the size range 0.05–1.50 μm radius. Note that these equations are valid only over the range of observed values of A to which they are fitted. The average error in an estimate of the cloud droplet concentration obtained using this parameterization can be given by the standard deviation of the points from the best-fit line, which for the maritime air masses is ± 19 cm^{-3} and for the continental air masses is ± 68 cm^{-3}.

2) CCN SUPERSATURATION SPECTRA BELOW CLOUD BASE

The relationship between the concentration of aerosol particles below cloud base and the concentration of CCN activated into cloud droplets will, for a particular airmass composition, depend not only on the actual proportion of aerosol that are CCN, but also on the relative values of the maximum in-cloud supersaturation and the critical supersaturation of the CCN (that is, the supersaturation at which the CCN are activated). The maximum supersaturation is largely dependent on the vertical updraft velocity: for stratocumulus clouds it is less than 0.8% because the updraft velocities are very small, and increases in supersaturation are rapidly reduced by condensation of water vapor onto cloud droplets. However, increases (or decreases) in the maximum supersaturation could cause increases (or decreases) in the number of CCN activated to cloud droplets within the same air mass, as illustrated by Twomey (1959).

In order to investigate the variations in the maximum supersaturation between the different stratocumulus layers studied here, CCN activity spectra measured just below cloud base were used. Activity spectra, typical examples of which are given in Fig. 9, show the CCN concentration activated at or below a particular supersaturation; this will obviously vary with the actual aerosol present. Provided there are no nonadiabatic processes occurring such as entrainment or drizzle, so that the droplet concentration in the cloud layer is the same as the concentration of CCN activated, it is possible to find the corresponding maximum supersaturation. Examples of CCN supersaturation spectra and the construction carried out to find the maximum in-cloud supersaturation are shown in Fig. 9 for both a maritime and a continental airmass case. This procedure for calculating the maximum supersaturation was carried out for all the CCN spectra measured below cloud base during the UK, FATE, and ASTEX flights (the instrument was not fitted during FIRE). Figure 10 shows how the maximum supersaturation varies from one stratocumulus sheet to another. Although there is considerable scatter in these results, the data for the continental air masses indicate that the maximum supersaturation for stratocumulus clouds is, on average, 0.35 $\pm$ 0.13% (one standard deviation). However, there is a linear trend in the data from the maritime air masses, indicating a greater sensitivity of the droplet concentration to changes in maximum supersaturation in these air masses. This implies a sensitivity to changes in vertical velocity. However, as discussed in the previous section, the small vertical velocities associated with stratocumulus clouds are extremely difficult to measure

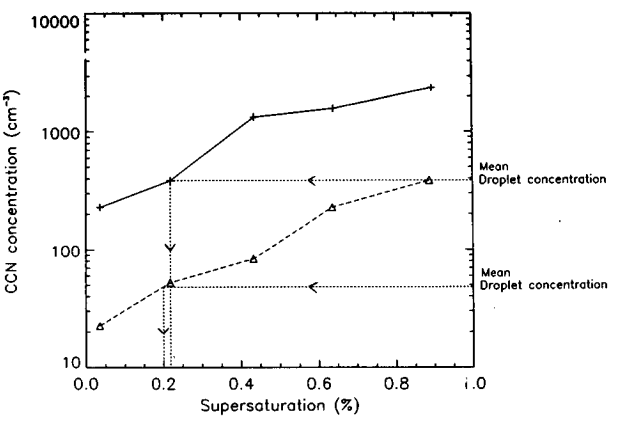

FIG. 9. CCN activity spectra measured just below cloud base in a continental air mass (solid line and crosses) during a flight over the North Sea on 7 February 1992 and a maritime air mass (dashed line and triangles) during ASTEX on 16 June 1992. The dotted line constructions show the procedure for estimating the maximum supersaturation encountered in the cloud from the mean cloud droplet concentration (cm^{-3}).

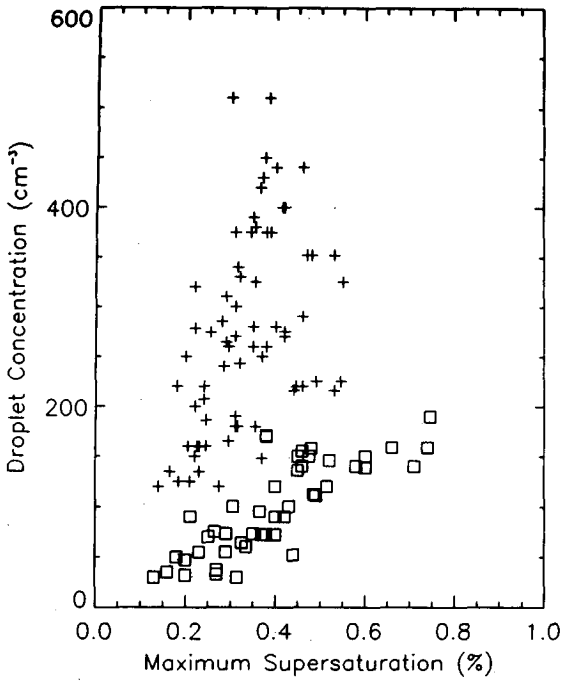

FIG. 10. Plot of cloud droplet concentration (cm^{-3}) against the estimated maximum supersaturation (%) for all the flights in which the CCN counter was fitted. Each point corresponds to a period where the CCN spectrum was measured just below a cloud sheet in which the droplet concentration was subsequently measured. Squares: maritime air masses; crosses: continental air masses.

with an aircraft, so it has not been possible to verify any relation to vertical velocity.

The results described above imply that, at least for a continental air mass in which stratocumulus clouds are forming, given the CCN activity spectrum and using a maximum in-cloud supersaturation of 0.35%, an estimate of the cloud droplet concentration, N_{TOT}, could be deduced and used in Eq. (11) to find the effective radius of the cloud droplets.

3) COMPARISON OF CCN AND AEROSOL SIZE SPECTRA

An alternative method of illustrating the difference between continental and maritime air masses is shown in Fig. 11. In each case, the CCN activity spectrum measured below cloud base (see Fig. 9) has been converted to a cumulative CCN size distribution using the Kohler equations (Pruppacher and Klett 1980), which relate CCN mass to supersaturation, and assuming a chemical composition of ammonium sulphate for the CCN (assuming different chemical compositions instead of ammonium sulphate altered slightly the shape of the cumulative CCN distribution but had little effect on the overall results). The cumulative PCASP size distribution is also plotted and it can be seen that for the maritime airmass case (Fig. 11a), the two graphs join together smoothly at $r = 0.05$ μm, where the fourth point from the CCN spectrum coincides with the first point from the PCASP. This implies that virtually all of the aerosol measured by the PCASP in maritime air masses are good CCN and are thus measured by the CCN counter. For the continental airmass case (Fig. 11b), the two graphs do not join together, and the cumulative particle concentration is much higher for the PCASP at $r = 0.05$ μm than for the CCN counter, since the PCASP is also measuring particles that are not CCN. The magnitude of this difference will thus depend on the chemical composition of the continental air mass. These results are in agreement with those shown in Fig. 8. However, the two spectra in Fig. 11b show a tendency to converge at extremely low radii (corresponding to water supersaturations exceeding ~0.8%), which shows that aerosol particles that were poor CCN at the typical supersaturation of 0.35% could be activated if the supersaturation rose sufficiently high. In both Figs. 11a and 11b, the data points from the CCN spectrum at a radius of 0.15 μm correspond to supersaturations below 0.04% and are thought to be in error due to end wall effects in the thermal gradient diffusion chamber, which are most marked at very low supersaturations (Saxena and Kassener 1970). Therefore, they show some discrepancies when compared with the shape of the PCASP spectrum and, generally, are ignored.

d. Effect of drizzle

The PMS two-dimensional cloud probe (2D-C) records a two-dimensional image of each droplet passing through it within the size range 25–800 μm diameter. The method of operation of this probe is described by Baumgardner (1989). A series of images can then be processed to yield a size spectrum of droplets passing through the probe during a specified time interval, so that spectra from different time intervals can represent different heights in cloud in the same way as the FSSP droplet size spectra.

Spectra for cloud droplets in this larger size range were calculated and combined with those from the FSSP to give complete size spectra from 2 to 800 μm, in order to assess the effects of the presence of drizzle drops on the overall spectral shape and on the parameterization of r_e. An example of this is given in Fig. 12a, where dN/dr has been plotted rather than N in order to remove the effect of varying channel widths between the two probes. It can be seen that the measurement ranges of the two probes overlap in the region 25–45.5 μm, so in order to create the single combined spectrum shown in Fig. 12b, the values from the 2D-C were interpolated onto the last seven size channels of the FSSP and the results averaged between the two probes. Bulk parameters such as the r_e could then be calculated for the whole spectrum.

In some cases, there were virtually no droplets large enough to be measured by the 2D-C, and in others the

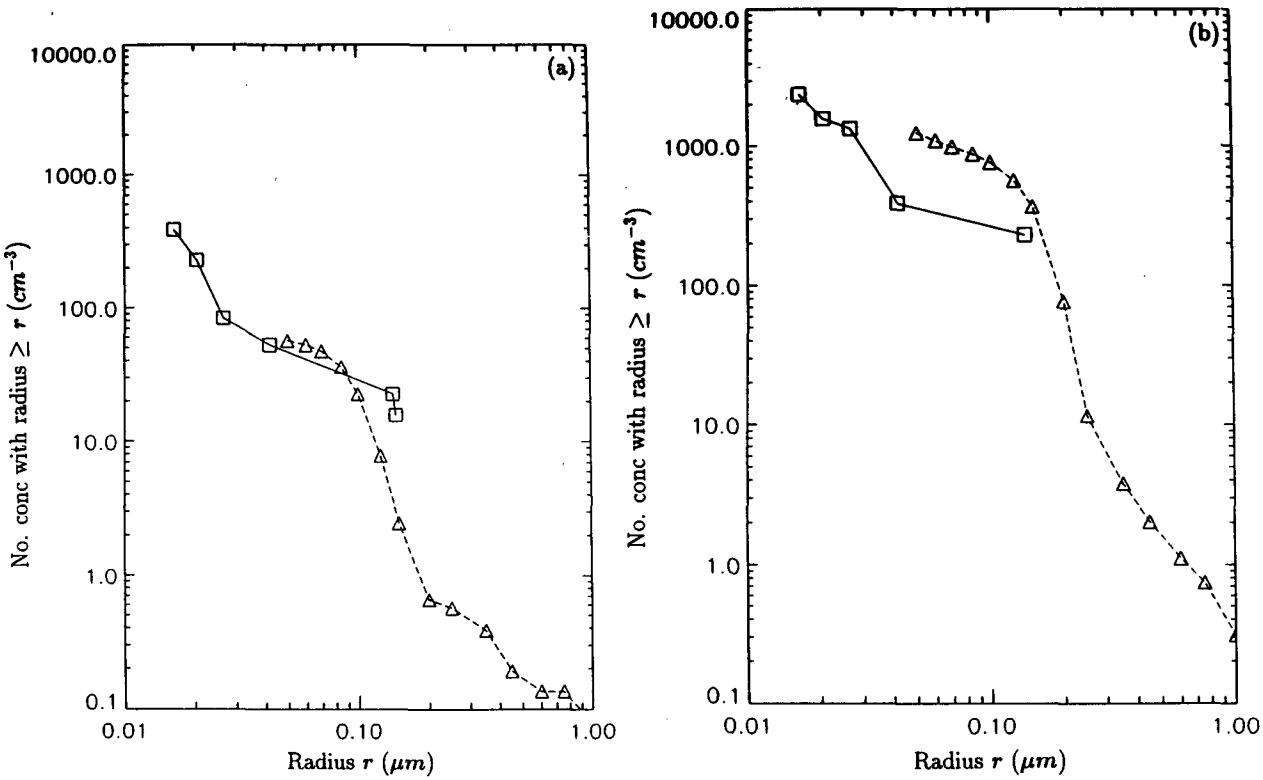

FIG. 11. Plot of cumulative particle size spectra as measured by the PCASP (dashed line and triangles) and determined from the CCN counter (solid line and squares) for (a) a maritime air mass in ASTEX on 16 June 1992 and (b) a continental air mass over the North Sea on 7 February 1992. The data points at a radius of 0.15 μm correspond to supersaturations below 0.04% and are thought to be in error due to end wall effects in the thermal gradient diffusion chamber (see text).

spectra were very narrow. However, on a number of occasions significant concentrations of droplets larger than 100-μm diameter were observed, particularly in maritime cases or when the cloud layer was extremely thick. In these cases, drizzle was usually observed to be falling from the base of the cloud, and it was even seen to reach the surface on one or two occasions. Figure 13a shows the combined spectra measured at different levels in and below cloud in a situation where there were large drops present but no drizzle was falling from the cloud base, and Fig. 13b shows data from a cloud layer that was drizzling. It can be seen that the change in spectral shape with height in cloud is different between the two cases. In the first case, the relative concentration of larger droplets increases toward the top of the cloud. However, in the drizzle case the reverse is true. Here, the droplets at cloud top have grown in size sufficiently for coalescence to be important as they fall through the cloud. Thus, the largest, drizzle-sized drops are found toward the cloud base, as is seen in Fig. 13b.

Values of r_e calculated using the combined spectra were compared with those from the FSSP spectra alone. It was found that in situations where the cloud is not drizzling, the inclusion of drops larger than 47 μm (the upper diameter range of the FSSP) has little effect on the overall spectral shape and so the r_e does not change greatly. In cases where the cloud layer is drizzling, the large numbers of drizzle drops in the lower half of the cloud contribute significantly to increasing the r_e at these levels. An example of this is given in Fig. 14 for the spectra shown in Fig. 12. However, the parameterization of r_e will only become invalid if the shape of the spectrum is modified in such a way by the presence of drizzle that the ratio of r_v^3 to r_e^3 (or k) is changed. Figure 15b shows how k changes in the drizzle case when the combined spectrum is used. Near the top of the cloud, where r_e and r_v are larger, the ratio is almost unchanged, but in the lower half of the cloud the ratio is significantly higher. However, in the nondrizzle case (Fig. 15a) it is virtually impossible to distinguish between the ratios derived from the combined spectra and those from the FSSP spectra alone. If an r_e is used in a shortwave radiation scheme, for optically thick clouds such as drizzling stratocumulus it is the droplets near the cloud top that determine the cloud's optical properties and must be parameterized correctly. Therefore, it is suggested that this parameterization of r_e can justifiably be applied to both nondrizzling and drizzling stratocumulus.

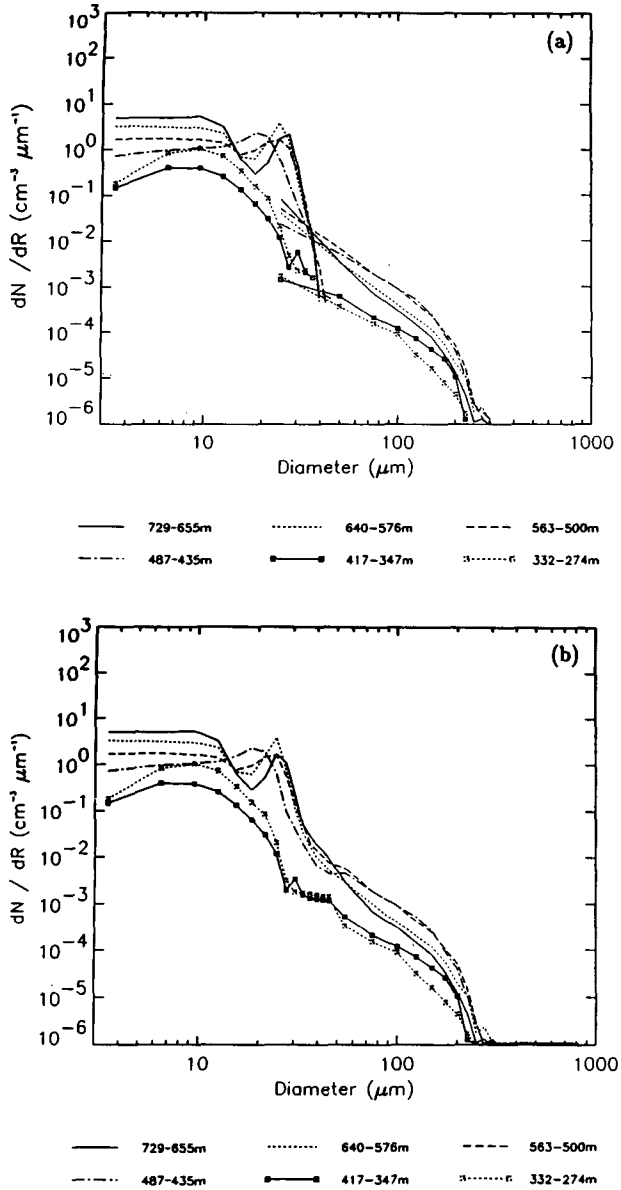

FIG. 12. Averaged droplet size spectra as measured by the FSSP and 2D-C probe in and just below a stratocumulus sheet during a profile in ASTEX on 16 June 1992 (a) showing the overlap region of the two spectra and (b) with the overlap region smoothed out. The main cloud layer extends from 435 to 729 m, with some scud below.

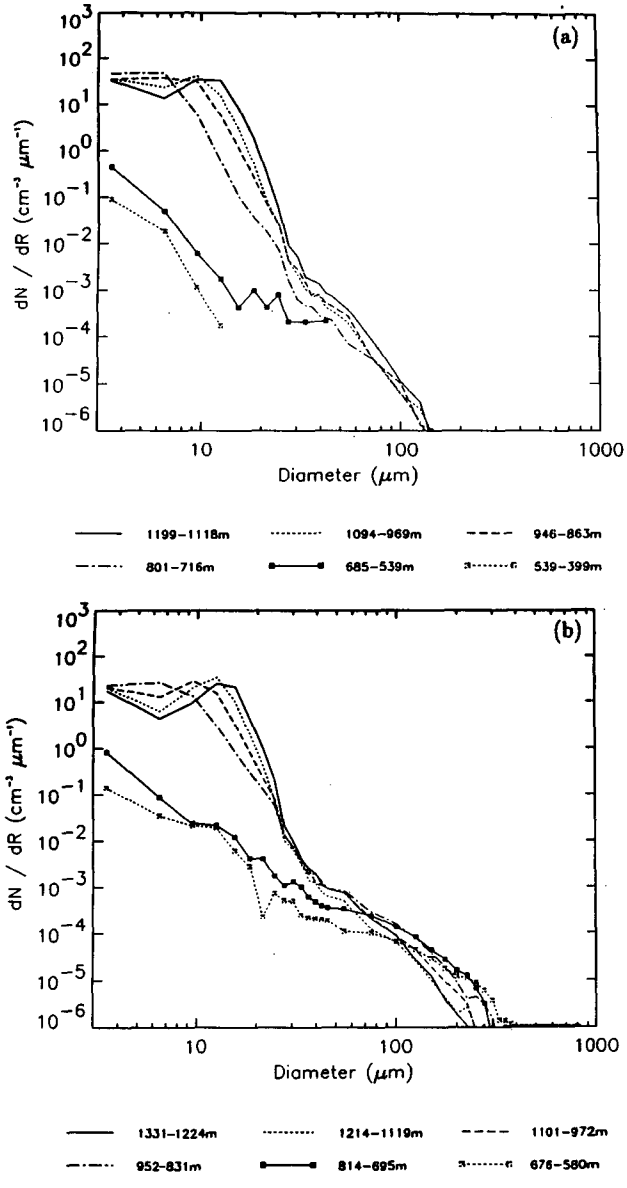

FIG. 13. Averaged droplet size spectra as measured by the FSSP and the 2D-C probe in and just below a stratocumulus sheet on a flight over the southwest approaches in a profile on 6 December 1990 in (a) an area of the cloud that is not drizzling (the main cloud layer extends from 716 to 1199 m) and (b) an area that is drizzling (the main cloud layer extends from 831 to 1331 m).

5. Conclusions and discussion

The measurements presented here of the microphysical properties of stratocumulus clouds and the aerosol characteristics of marine boundary layers from several regions around the globe have enabled us to produce a parameterization of effective radius of layer clouds for radiation schemes in large-scale numerical models. In general, the observations have been taken from relatively homogeneous clouds where entrainment processes such as cloud-top entrainment instability (McVean and Mason 1990) and penetration by cumulus clouds are negligible or insignificant. In these circumstances, r_e^3 was found to be a linear function of r_v^3. Therefore, it has been possible to relate the r_e to the liquid water content and droplet concentration in the cloud. It was also found that the droplet concentration can be parameterized in terms of the aerosol concentration if the origin of the air mass is known.

During the course of this work it was found that the most suitable parameterization for effective radius of droplets in layer clouds is

$$r_e\,[\mu\text{m}] = 10^3\left(\frac{3L\,[\text{g m}^{-3}]}{4\pi\rho_w k N_{\text{TOT}}\,[\text{cm}^{-3}]}\right)^{1/3}, \quad (14)$$

where the values of k and N_{TOT} are

(i) in maritime airmasses:

$$k = 0.80 \pm 0.07 \text{ (1 standard deviation)}$$

$$N_{\text{TOT}} = -1.15 \times 10^{-3}A^2 + 0.963A + 5.30, \quad (15)$$

where A is the aerosol concentration in the range ($36 \leq A \leq 280$ cm^{-3}) and

(ii) in continental air masses:

$$k = 0.67 \pm 0.07 \text{ (1 standard deviation)}$$

$$N_{\text{TOT}} = -2.10 \times 10^{-4}A^2 + 0.568A - 27.9 \quad (16)$$

for values of A in the range ($375 \leq A \leq 1500$ cm^{-3}).

Figure 16 shows a comparison, from the UK, FATE, and ASTEX flights, of the observed r_e and the predicted r_e from the parameterization using measurements of the liquid water and aerosol concentration from below cloud base. The $y = x$ line is marked on and the dashed and dash–dot lines indicate the r_e value that currently is being used in the U.K. Meteorological Office unified model and the ECMWF operational model, respectively. In general, the parameterization is performing well and, as would be expected, is a much better indicator of r_e than using a constant value.

When entrainment effects become important, the relationship between r_e and r_v breaks down and such data have been ignored in the analysis. Figure 17a shows an example of a scatterplot of r_e^3 against r_v^3 during a profile in a situation where other measurements show that entrainment was taking place (or had taken place) at cloud top. Throughout three-quarters of the depth of the cloud the linear relationship holds, but in the top quarter the points are very scattered and r_e is larger than expected. When cumulus clouds are affecting a stratocumulus layer the results are far more unpredictable. Figures 17b and 17c show two examples of this. In both cases an extensive sheet of stratocumulus was observed, with large amounts of cumulus below it that had formed at the top of a decoupled surface mixed layer. Several of the cumulus clouds were seen penetrating the base of the stratocumulus. In Fig. 17b, the gradient of the scatterplot changes during the profile. The points with the lower r_e, which are in the lower part of the cloud layer, appear to be associated with the aircraft flying through the top part of a cumulus cloud embedded in the base of the stratocumulus. Because of the different entrainment processes involved with the dynamics of cumulus and stratocumulus clouds, the spectral shapes are generally quite different for the two types and can be used as a tracer for convective parcels

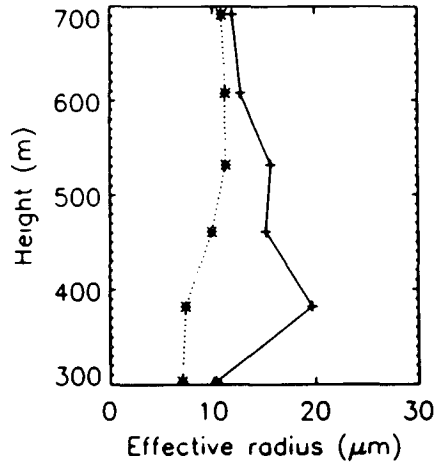

FIG. 14. A vertical profile of r_e (μm) calculated from droplet spectra measured by the FSSP alone (dotted line) and measured by the FSSP and 2D-C combined (solid line). The droplet spectra used are the ones shown in Fig. 12.

penetrating the stratocumulus layer. Obviously, as more and more mixing occurs between them the ability to do this decreases. The points with higher r_e in Fig. 17b may represent growth of a droplet spectrum that has been formed where stratocumulus and cumulus parcels have mixed more thoroughly. In the second case of a cumulus penetration (Fig. 17c) the change in the characteristics of the scatterplot between the cumulus and the stratocumulus is more marked. Once again the cumulus cloud was encountered in the lower half of the cloud and the spectra have smaller r_e there. The points are more scattered and there is a sharp change as the aircraft flies out of the active cumulus and into the modified stratocumulus.

It became clear during the course of this work that to be able to parameterize the microphysical properties of stratocumulus correctly, in particular r_e, the aerosol characteristics below cloud base had to be considered. Therefore, we feel it is essential that more large-scale numerical models start to incorporate algorithms for the prediction of advection, sources, and sinks of aerosol so that the cloud–climate feedback processes can be handled more accurately. It is also essential that models label continental and maritime air masses in a better way. Many continental air masses can maintain their characteristics for several days and for several thousands of kilometers over a sea surface. This is important as clouds within continental air masses have the potential to have much higher albedos than clouds within maritime air masses.

The variation in the factor k between maritime and continental airmass cases is caused by the fundamental difference in spectral shape highlighted in section 3. It is instructive to relate k to statistical descriptions of spectral shape such as spectral dispersion and the co-

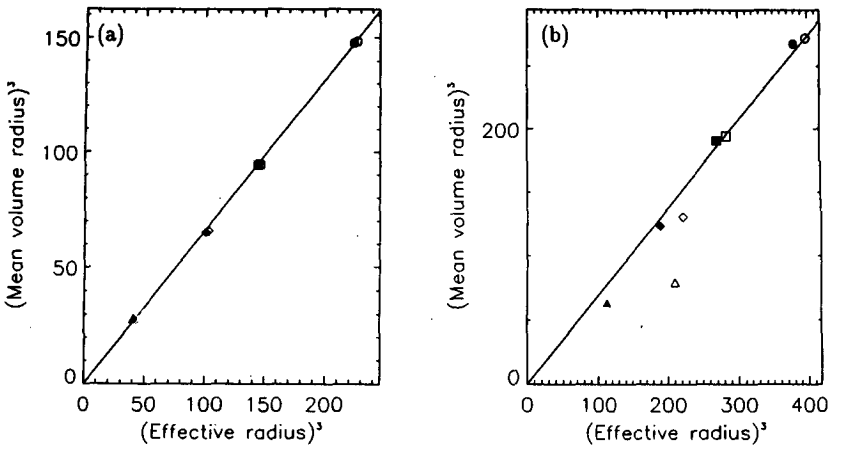

FIG. 15. Plots of r_v^3 (μm^3) against r_e^3 (μm^3) in profiles on 6 December 1990 over the southwest approaches of the British Isles calculated from FSSP spectra alone (solid data points) and FSSP and 2D-C spectra combined (open data points) for (a) a sheet of stratocumulus that was not drizzling (circle: 1118–1199 m, square: 969–1094 m, diamond: 863–946 m, and triangle: 716–801 m) and (b) one that was drizzling (circle: 1224–1331 m, square: 1119–1214 m, diamond: 972–1101 m, and triangle: 831–952 m). Solid line is best fit line to FSSP spectra alone. The spectra used are the same as those shown in Fig. 13.

efficient of skewness. This may be done by writing k in the form

$$k = \frac{(\overline{r^2})^3}{(\overline{r^3})^2}, \tag{17}$$

using Eqs. (4), (9), and (10).

Following the method of Pontikis and Hicks (1992), $(\overline{r^2})^3$ can be expressed in terms of dispersion by expanding the equation for standard deviation:

$$\sigma = \left(\frac{1}{N_T}\int_0^\infty (r - \bar{r})^2 dr\right)^{1/2}, \tag{18}$$

where N_T is the total number of droplets in the spectrum, and using Eq. (5), so that

$$(\overline{r^2})^3 = [\bar{r}^2(1 + d^2)]^3. \tag{19}$$

An expression for $(\overline{r^3})^2$ can be derived using the equation for the coefficient of skewness a:

$$a = \frac{1}{\sigma^3 N_T}\int_0^\infty (r - \bar{r})^3 dr \tag{20}$$

so that

$$(\overline{r^3})^2 = [\bar{r}^3(ad^3 + 1 + 3d^2)]^2. \tag{21}$$

Equation (17) can now be used to give the following expression for k:

$$k = \frac{(1 + d^2)^3}{(ad^3 + 1 + 3d^2)^2}. \tag{22}$$

Figure 18 shows how k varies with dispersion for several values of a. In all cases, k decreases to a minimum value that is strongly dependent on a. The value of d at which this occurs is also dependent on a, and is less than one for $a < 0$ and greater than one for $a > 0$. It is interesting to notice that it is possible for k to be greater than one (that is, r_v is larger than r_e), and that this will occur at successively lower values of d as the skewness decreases. Also shown on the diagram are the values of k for the maritime and continental airmass cases as given in Eqs. (14) and (17). Typical values of spectral dispersion measured in maritime and continental airmass cases during this study are also indi-

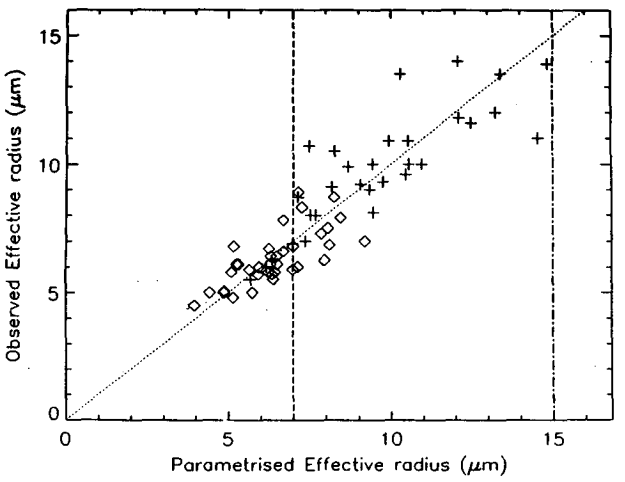

FIG. 16. A comparison of observed r_e (μm) and the predicted r_e (μm) from the parameterization. Dotted line is $y = x$, the dashed line indicates the single value of r_e used in the U.K. Meteorological Office unified model, and the dash–dot line is the single value of r_e used in the ECMWF operational model. Diamonds and crosses indicate continental and maritime airmass data points, respectively, from the FATE, ASTEX, and UK experiments.

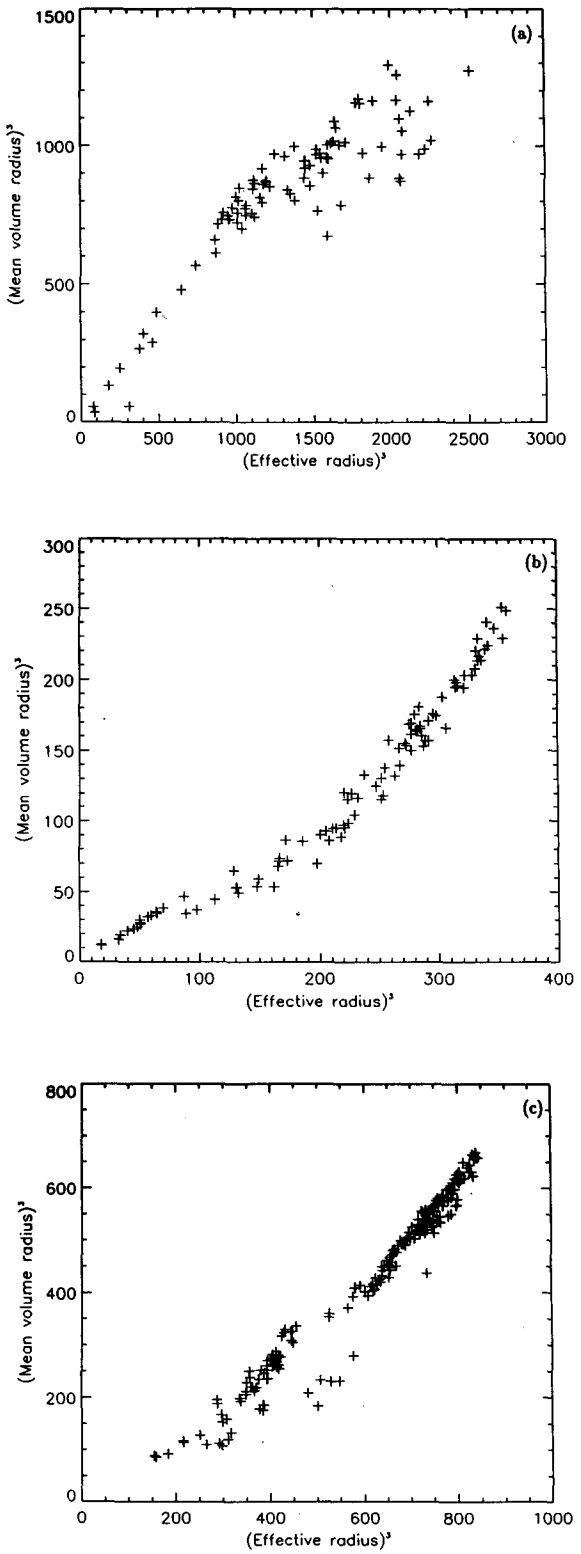

FIG. 17. Scatterplots of r_v^3 against r_e^3 showing the effects of (a) entrainment at cloud top during a profile in ASTEX on 16 June 1992, (b) and (c) cumulus clouds penetrating the base of the stratocumulus in a profile over the North Sea on 18 May 1990 and an ASTEX flight on 19 June 1992, respectively.

cated. It can be seen that for the majority of the continental airmass cases, the coefficient of skewness is positive, and for most of the maritime cases it is negative. However, for these values of dispersion, $a = 0$ may be a fair approximation, especially since k will be affected much more by changes in dispersion than changes in coefficient of skewness because of the d^6 terms in Eq. (22). This approximation reduces Eq. (22) to the following expression:

$$k = \frac{(1 + d^2)^3}{(1 + 3d^2)^2}. \tag{23}$$

Thus, the parameterization of effective radius given in Eq. (13) may also be written

$$r_e = \left(\frac{3L(1 + 3d^2)^2}{4\pi\rho_w N_{\mathrm{TOT}}(1 + d^2)^3}\right)^{1/3}, \tag{24}$$

where $d = 0.33 \pm 0.08$ (1 standard deviation) for maritime air masses, and $d = 0.43 \pm 0.06$ for continental air masses. Figure 19 shows a comparison of observed and parameterized r_e using Eq. (24). It can be seen that the assumption of $a = 0$ has only a small effect on the parameterized values compared with Fig. 16, making the parameterized maritime airmass values slightly larger and the parameterized continental airmass values slightly smaller.

Pontikis and Hicks (1992) derived a parameterization for r_e in terms of spectral dispersion for use in cumulus clouds, which contains a factor $F(d)$ that is equivalent to $k^{-1/3}$ and uses the assumption $\overline{(r - r)^3} = 0$, that is, that the coefficient of skewness is zero. On applying their parameterization to cumulus clouds measured during the JHWRP in very clean maritime air masses, they found that $F(d)$ had an average value of 1.05, which corresponds to $k = 0.86$, and (from Fig. 18) to $d = 0.24$. This is just outside the region indicated by our results for maritime airmass cases and indicates that cumulus clouds such as those sampled in JHWRP have slightly different microphysical characteristics 2from the stratocumulus clouds investigated in this study, as would be expected due to the higher entrainment rates associated with cumulus clouds. However, these results imply that Eq. (14) may be used in a numerical model as a parameterization of effective radius in stratocumulus and cumulus clouds, provided that the appropriate value of k is used. Further work will be required to determine typical values of k in, for example, continental cumulus clouds.

Other parameterizations of r_e were discussed briefly in the introduction. Figure 20a–c shows comparisons of r_e calculated using each of these parameterizations with the observed r_e values measured during this study. The Canadian Climate Centre model parameterizes r_e in terms of liquid water content using Eq. (2). Figure 20a shows that this parameterized r_e agrees well with the observed values for continental air masses, but that r_e in the maritime airmass clouds is often significantly

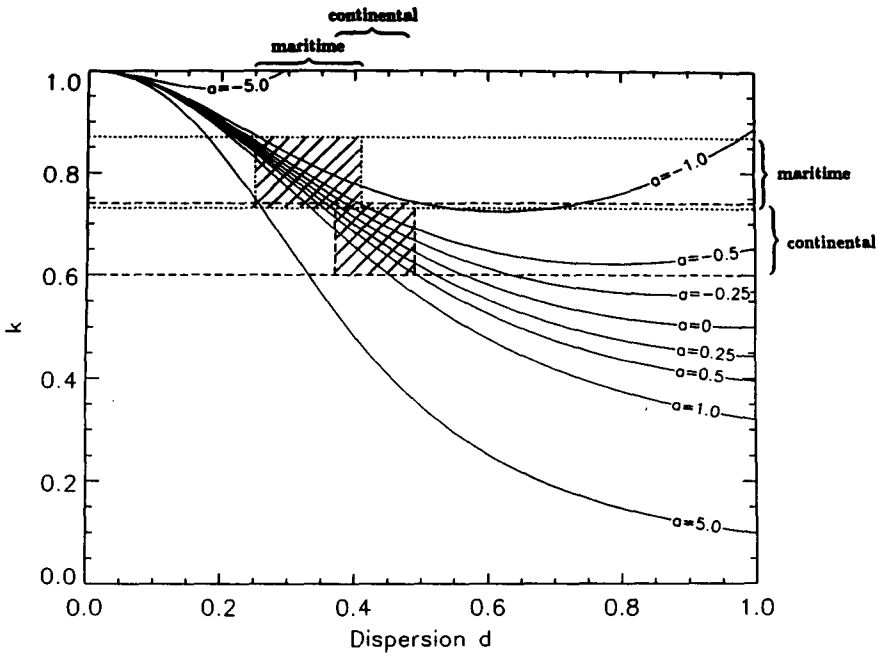

FIG. 18. A plot of the variation of k against dispersion (d) for several values of the coefficient of skewness (a). Shaded regions indicate the average values ± 1 standard deviation of k and d for the continental and maritime airmass clouds observed during all the experiments.

underestimated by the parameterization. This is likely to be the result of only allowing a dependence on liquid water content, which may be the same in two boundary layers that have different aerosol concentrations and will therefore produce clouds with different droplet sizes. Figure 20b shows the parameterization of Moeng and Curry (1990), which was derived using the drop size distribution described in Eq. (3) to give the following equation for r_e:

$$r_e = \frac{5}{b}, \tag{25}$$

where

$$b = (2.094395 \times 10^5 N/q_l)^{1/3} \tag{26}$$

and

$$N = 50 + 700 \times 10^3 q_l - 300 \times 10^6 q_l^2. \tag{27}$$

In these equations, q_l is liquid water mixing ratio (kg/kg) and N is droplet concentration (cm^{-3}). Equation (27) was determined empirically from observations of arctic stratus clouds. It can be seen from Fig. 20b that this parameterization significantly underestimates the variation of r_e found in our measurements. This is likely to be a result of the assumed drop size distribution, which Moeng and Curry state may be too broad for subtropical marine stratus. Also, errors may be caused by our use of this parameterization of N, which is based on arctic stratus cloud data, for marine stratocumulus.

Figure 20c shows the parameterization of Bower and Choularton (1992) for r_e in stratocumulus clouds, which states that

$$r_e = 100 \times \left(\frac{3L}{4\pi N}\right)^{1/3}, \tag{28}$$

where L is liquid water content (in g m^{-3}) and N is a

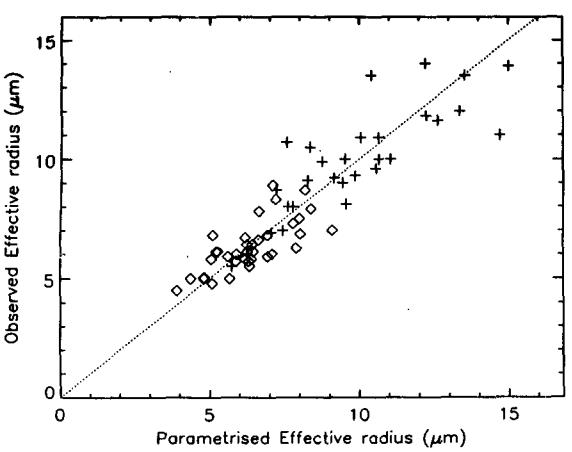

FIG. 19. Comparison of observed r_e (μm) and parameterized r_e (μm) assuming the coefficient of skewness of all the droplet size spectra is 0. Diamonds and crosses indicate continental and maritime airmass data points, respectively, from the FATE, ASTEX, and UK experiments. Dotted line is $y = x$.

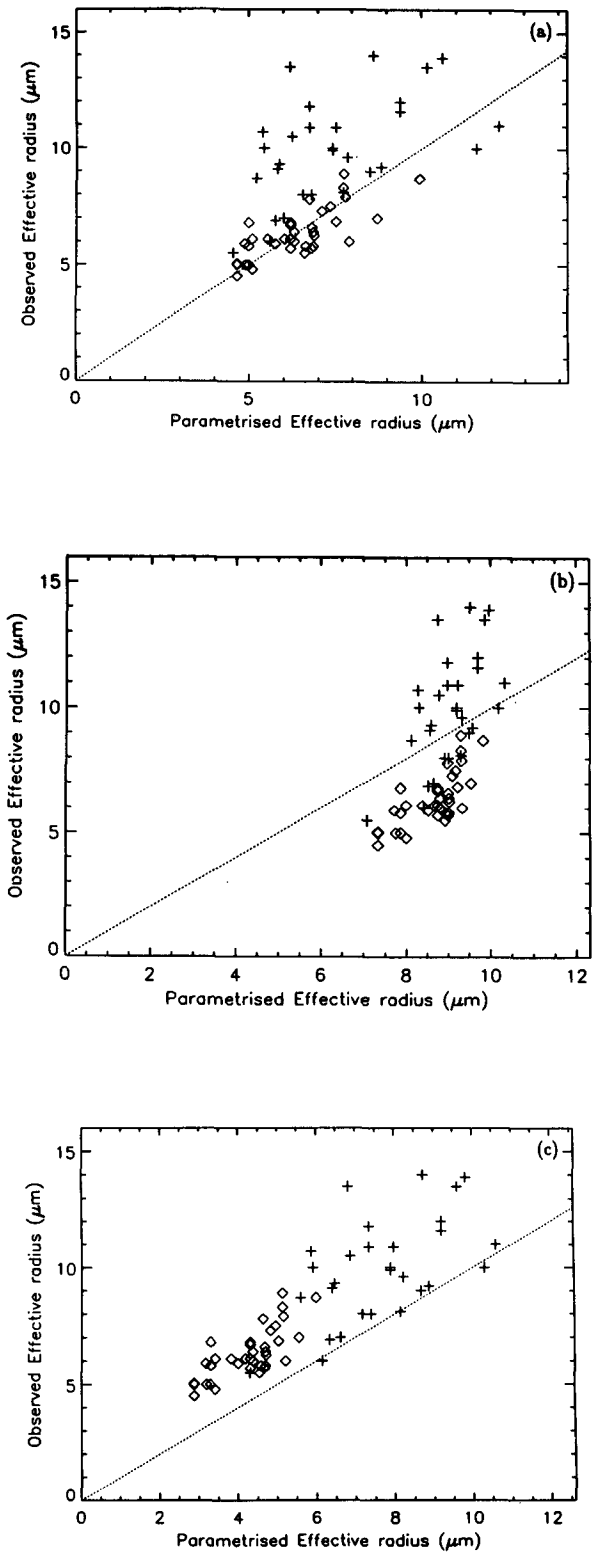

FIG. 20. Comparisons of observed r_e (μm) with parameterizations of r_e (μm) used by (a) the Canadian Climate Centre model, (b) Moeng and Curry, and (c) Bower and Choularton. Diamonds and crosses indicate continental and maritime airmass data points, respectively, from the FATE, ASTEX, and UK experiments.

fixed value of 150 cm^{-3} over the oceans and 600 cm^{-3} over the continents. Although all the clouds in our study were over the oceans, the continental or maritime division used throughout this paper was employed with the Bower and Choularton parameterization. They suggest that L is the liquid water content predicted by the general circulation model cloud scheme, which would be close to the adiabatic value in these clouds. For the purposes of this comparison, the measured FSSP liquid water content has been used. This parameterization consistently underestimates r_e in both types of air mass, mainly as a result of the high droplet concentration used in each case, compared with typical values measured with the FSSP in this study (see Fig. 8), and also because the parameterization assumes that $k = 1$.

The parameterization of the droplet concentration in layer clouds in continental air masses is probably the weakest point of our parameterization of r_e. Due to the large diversity of the chemical characteristics of the CCN and aerosol produced over the land, the degree of correlation between aerosol concentration and cloud droplet concentration is not as high as we would wish. This could be improved if more data were collected and analyzed from specific continental source regions such as highly industrialized regions, deserts, or arboreal areas. Then source-specific parameterizations of N_{TOT} could be developed and a numerical model could base its decision of which to use on the location of the source.

Until now, very little work has been done on categorizing the chemical composition of the aerosol we have been sampling in the boundary layer. Similarly, no flights have been made in stratocumulus over land, in highly polluted air masses where the aerosol concentration is greater than 1500 cm^{-3}. Future work should try to rectify this. From satellite observations and measurements made during this work it is clear that the interaction of cumulus clouds and stratocumulus layers has a modifying effect on the reflectivity of the stratocumulus especially in the subtropics and in the late afternoon in midlatitudes. Currently, we are investigating how this parameterization could be modified to allow for the incursion and mixing of parcels of cloudy air having typical cumulus droplet size spectra into layers of stratocumulus. This will be reported on in future papers.

Acknowledgments. We would like to thank the scientists and Royal Air Force crew of the MRF, without whose dedicated support this work would not have been possible. In particular, the pilots, Sqn. Ldr. Martin Lampitt and Sqn. Ldr. Harry Burgoyne, during their periods of Officer in Command at MRF, were exceedingly helpful and patient with our eccentric requests. We would also like to thank P. R. A. Brown for many useful discussions on the operation and analysis of data from the FSSP and 2D-C probe, and Dr. G. J. Jenkins for his continued encouragement and constructive crit-

icism of this work. Gill Martin was supported by a consortium of oil companies within the International Petroleum Industry Environment Conservation Association (IPIECA).

REFERENCES

Albrecht, B. A., D. A. Randall, and S. Nicholls, 1988: Observations of marine stratocumulus during FIRE. *Bull. Amer. Meteor. Soc.*, **69,** 618–626.

Baumgardner, D., 1983: An analysis and comparison of five water droplet measuring instruments. *J. Appl. Meteor.*, **22,** 891–910.

——, 1989: Airborne measurements for cloud microphysics. NCAR Research Aviation Facility Bulletin No. 24, NCAR [P.O. Box 3000, Boulder, CO 80307].

——, and M. Spowart, 1990: Evaluation of the Forward Scattering Spectrometer Probe. Part III: Time response and laser inhomogeneity limitations. *J. Atmos. Oceanic Technol.*, **7,** 666–680.

Betts, A. K., and R. Boers, 1990: A cloudiness transition in a marine boundary layer. *J. Atmos. Sci.*, **47,** 1480–1497.

Blyth, A. M., and J. Latham, 1991: A climatological parameterization for cumulus clouds. *J. Atmos. Sci.*, **48,** 2367–2371.

Bower, K. N., and T. W. Choularton, 1992: A parametrisation of the effective radius of ice free clouds for use in global climate models. *Atmos. Res.*, **27,** 305–339.

Charlson, R. J., J. E. Lovelock, M. O. Andreae, and S. G. Warren, 1987: Ocean phytoplankton, atmospheric sulphur, cloud albedo and climate. *Nature,* **326,** 655–661.

Cooper, W. A., 1988: Effects of coincidence on measurements with a Forward Scattering Spectrometer Probe. *J. Atmos. Oceanic Technol.,* **5,** 823–832.

Curry, J. A., and G. F. Herman, 1985: Infrared radiative properties of summertime arctic stratus clouds. *J. Climate Appl. Meteor.,* **24,** 525–538.

Fouquart, Y., J. C. Buriez, M. Herman, and R. S. Kandel, 1990: The influence of clouds on radiation: A climate-modelling perspective. *Rev. Geophys.,* **28,** 145–166.

Golding, B. W., 1990: The Meteorological Office Mesoscale Model. *Meteor. Mag.,* **119,** 81–96.

Jonas, P., 1990: On the parametrization of clouds containing water droplets. *Quart. J. Roy. Meteor. Soc.,* **117,** 257–263.

Langner, J., H. Rodhe, P. J. Crutzen, and P. Zimmermann, 1992: Anthropogenic influence on the distribution of tropospheric sulphate aerosol. *Nature,* **359,** 712–715.

McFarlane, N. A., G. J. Boer, J.-P. Blanchet, and M. Lazare, 1992: The Canadian Climate Centre second-generation general circulation model and its equilibrium climate. *J. Climate,* **5,** 1013–1044.

McVean, M. K., and P. J. Mason, 1990: Cloud-top entrainment instability through small-scale mixing and its parameterization in numerical models. *J. Atmos. Sci.,* **47,** 1012–1030.

Mitchell, J. F., C. A. Senior, and W. J. Ingram, 1989: CO_2 and climate: A missing feedback? *Nature,* **341,** 132–134.

Moeng, C.-H., and J. Curry, 1990: The sensitivity of large eddy simulations of a stratus topped boundary layer to cloud microphysics. *Proc. Conf. on Cloud Physics,* San Francisco, Amer. Meteor. Soc., 115–121.

Morcrette, J-J., 1990: Impact of changes to the radiation transfer parametrisations plus cloud optical properties in the ECMWF model. *Mon. Wea. Rev.,* **118,** 847–873.

Nicholls, S., 1978: Measurements of turbulence by an instrumented aircraft in a convective boundary layer over the sea. *Quart. J. Roy. Meteor. Soc.,* **104,** 653–676.

——, 1984: The dynamics of stratocumulus: Aircraft observations and comparisons with a mixed layer model. *Quart. J. Roy. Meteor. Soc.,* **110,** 783–820.

——, and J. Leighton, 1986: An observational study of the structure of stratiform cloud sheets: Part I. Structure. *Quart. J. Roy. Meteor. Soc.,* **112,** 431–460.

Perkins, P., and U. R. C. Gustafsson, 1975: An automated atmospheric sampling system operating on 747 airliners. NASA Tech. Paper TM-X 71790.

Pontikis, C. A., and E. M. Hicks, 1992: Contribution to the cloud droplet effective radius parametrisation. *Geophys. Res. Lett.,* **19,** 2227–2230.

Pruppacher, H. R., and J. D. Klett, 1980: *Microphysics of Clouds and Precipitation.* D. Reidel, 141–142.

Randall, D. A., J. A. Coakley Jr., C. W. Fairall, R. A. Kropfli, and D. H. Lenschow, 1984: Outlook for research on subtropical marine stratiform clouds. *Bull. Amer. Meteor. Soc.,* **65,** 1290–1301.

Saxena, V. K., and J. L. Kassener Jr., 1970: Thermal-diffusion chambers as cloud-nuclei counters. *Proc. U.S. Atomic Energy Commission Symp. on Precipitation Scavenging,* Washington, NTIS CONF-700601, 217–238.

Schmetz, J., A. Slingo, S. Nicholls, and E. Raschke, 1983: Case studies of radiation in the cloud-capped atmospheric boundary layer. *Philos. Trans. Roy. Soc. London,* **308,** 377–388.

Slingo, A., 1989: A GCM parameterization for the shortwave radiative properties of water clouds. *J. Atmos. Sci.,* **46,** 1419–1427.

——, 1990: Sensitivity of the earth's radiation budget to changes in low clouds. *Nature,* **343,** 49–51.

——, and H. M. Schrecker, 1982: On the shortwave radiative properties of stratiform water clouds. *Quart. J. Roy. Meteor. Soc.,* **108,** 407–426.

Stephens, G. L., 1978a: Radiation profiles in extended water clouds. I: Theory. *J. Atmos. Sci.,* **35,** 2111–2122.

——, 1978b: Radiation profiles in extended water clouds. II: Parametrization schemes. *J. Atmos. Sci.,* **35,** 2123–2132.

Strapp, J. W., W. R. Leaitch, and P. S. K. Liu, 1992: Hydrated and dried aerosol-size-distribution measurements from the Particle Measuring Systems FSSP-300 probe and the deiced PCASP-100X probe. *J. Atmos. Oceanic Technol.,* **9,** 548–555.

Taylor, K. E., and S. J. Ghan, 1992: An analysis of cloud liquid water feedback and global climate sensitivity in a general circulation model. *J. Climate,* **5,** 907–919.

Twomey, S., 1959: The nuclei of natural cloud formation: The supersaturation in natural clouds and the variation of cloud droplet concentrations. *Geophys. Pura Appl.,* **43,** 243–249.

——, 1974: Pollution and the planetary albedo. *Atmos. Environ.,* **8,** 1251–1256.

——, 1977: The influence of pollution on the shortwave albedo of clouds. *J. Atmos. Sci.,* **34,** 1149–1152.